SLAC – PUB – 3829
November 1985
T/E

Review of Recent Progress in the Development of Čerenkov Ring Imaging Detectors*

David W.G.S. Leith

Stanford Linear Accelerator Center
Stanford University, Stanford, California 94305

1. INTRODUCTION

In the late 1970's Ypsilantis and Seguinot[1] proposed an extension of the classic binary "yes/no" Čerenkov counter to a new kind of particle identification system, with large dynamic range, robust performance and the potential to perform in the "heavy traffic" of the multi-particle jet environment. These new detectors were called Ring Imaging Čerenkov (RICH) counters[2] or Čerenkov Ring Imaging Detectors (CRIDs).[3]

The principle behind these devices involves focussing the Čerenkov light, emitted by a relativistic charged particle in passing through a radiator medium, onto a high efficiency photocathode which can in turn be read out with good spatial resolution, to localize the point of origin of the photoelectrons. This information permits the reconstruction of the circle of Čerenkov light for each particle above threshold, and hence the determination of the Čerenkov angle to an accuracy of a few percent. These principles are outlined in Figures 1(a)-(c).

* Work supported by the Department of Energy under contract No. DE-AC03-76SF00515.

Invited talk presented at the Annual Meeting of the Division of Particles and Fields of the APS, Eugene, Oregon, August 12-15, 1985

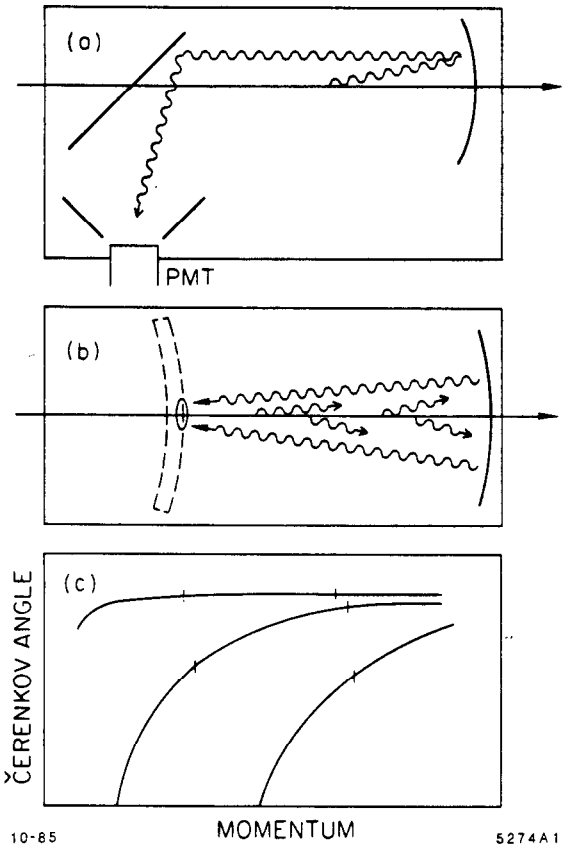

Fig. 1 Schematic representation of (a) a classic threshold counter, (b) a ring imaging detector, and (c) the separation of different species of particles through measurement of the Čerenkov angle.

However, there are a number of rather basic problem areas that have to be addressed before one can proceed with plans to implement a large ring imaging device.

- Photocathode:
  - — The photocathode has to be very efficient, since for practical geometries the radiator dimensions are such that only a few dozen Čerenkov photons are produced.
  - — The area of realistic photocathode surfaces tend to be large–of order of a few square meters to a few tens of square meters.
  - — The photocathode should be capable of being read out electronically with pixell size of order 1 mm^3.

- Detectors:
  - The detectors have to be capable of efficiently detecting single photoelectrons and must have some protection from photon feedback.

    Photon feedback is the positive feedback phenomenon caused when a very efficient photoionizing agent is placed close to a MWPC which causes light emission from the electron avalanche near the anode wires.
- High Purity Fluid Systems:
  - At the wavelengths one chooses to work, a few parts per million of oxygen or water vapor in any of the gas or liquid systems would attenuate the Čerenkov light and the photoelectrons. Care has to be taken to use clean construction materials and to recirculate the fluids through filters.
- Mirror System:
  - The optical arrangement in most Čerenkov ring imaging devices requires large area mosaics of quartz or calcium fluoride window arrays to separate the photocathode gas from the radiator gas, and rather large area arrays of mirrors with good reflectance (*i.e.*, $> 75\%$) in the vacuum ultraviolet wavelength region.

Given acceptable solutions to these problems one should expect superior performance from a Čerenkov ring imaging particle identification system. An example, taken from the SLD Design Report[4] is shown in Fig. 2.

For the remainder of this talk we will look at which groups are currently working on these new detectors, examine the status of these projects and report in some detail on the recent R&D progress from the two 4π devices being prepared for physics at the Z^0.

2. WHO ARE IN THE GAME?

There are four different collaborations actively working on the implementation of large Čerenkov ring imaging devices. I will briefly describe each of the detectors and their status.

2.1 E605 At Fermilab

This is a forward spectrometer experiment in the fixed target program at Fermilab, designed to study very high energy hadron-hadron collisions. The best known result of this experiment is probably the spectacular dimuon mass spectrum produced in 800 GeV proton-nucleus collisions, but the spectrometer is equipped with a sophisticated ring imaging counter to provide π, K, p identification of secondary hadrons up to around 200 GeV/c.[5] A schematic of their

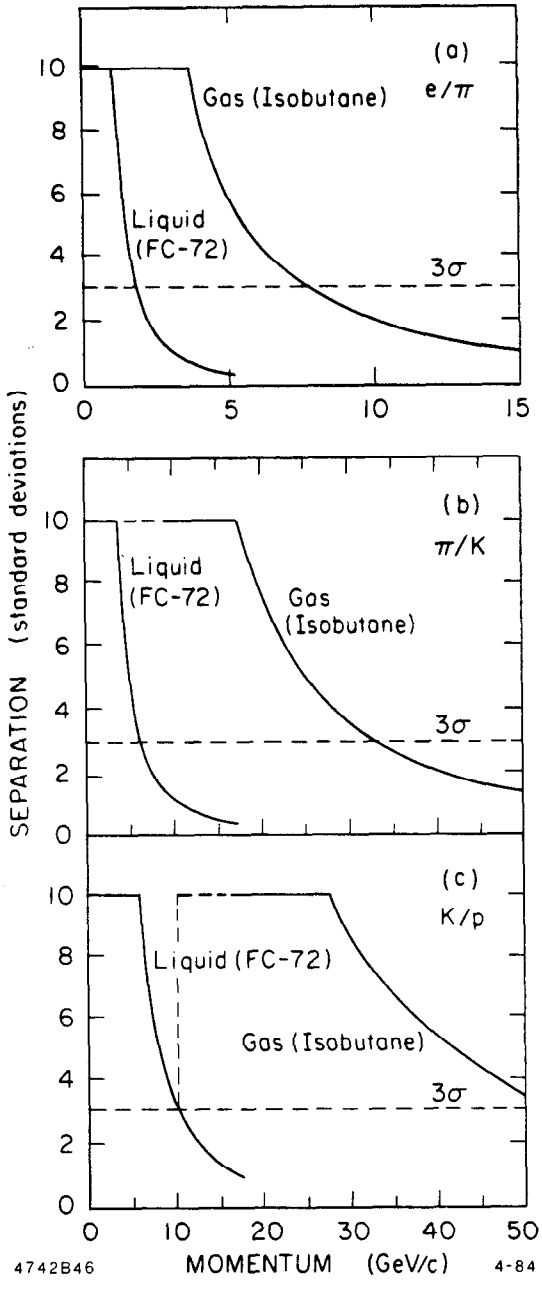

Fig. 2 The particle identification capability for a two radiator CRID, such as described in Ref. 4. The performance of the liquid (FC-72) and gas (isobutane) radiators is shown separately. The dashed line indicates the region where the heavier particle is below threshold. The separation is cut-off at 10 σ, under the assumption that tails in measurement error distributions make it unrealistic to quote such large separations. The separation is shown for (a) e/π, (b) π/K and (c) K/p.

RICH is shown in Fig. 3. The radiator is 15 meters of gaseous helium, and the Čerenkov light produced in this radiator is focused back onto the photon detectors by an array of 16 spherical mirrors. The detectors are isolated from the radiator volume by a mosaic of CaF_2 windows–each 4 mm thick and 10×10 cm^2 in area. The mirror reflectance is measured to be greater than 75% down to wavelengths of 150 nm, and over the same wavelength range the window transmission is measured to be greater than 70%. Each detector measures (40×80) cm^2 in size, and is mounted one on each side of the radiator volume (see Fig. 3).

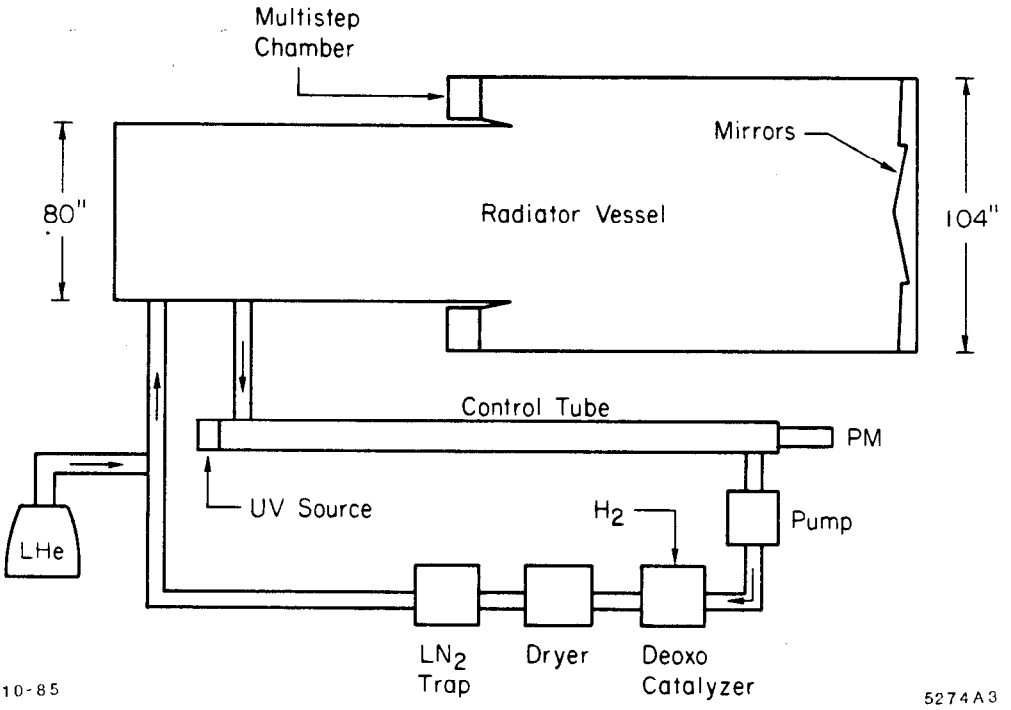

Fig. 3 Schematic of the Fermilab E-605 experiment ring imaging counter. See Ref. 5 for details.

The detector works by converting the Čerenkov light to free electrons via photoionization of an admixture of timethylamine (TEA) to the detector gas mixture. The photoelectron then drifts under the action of electric field to a preamplification gap and then onto a multiwire proportional chamber. A schematic of the electro-static grid structure is given in Fig. 4. The detector gas mixture is 90 : 5 : 3 of helium : methane : triethylamine, (TEA). The absorption length for the vacuum U.V. Čerenkov light in this gas mixture is of order 1 mm. The total gain of the preamplification gap and the narrow gap PWC is about 10^7. The PWC anode is constructed of 20 μm wires wound on a 2 mm pitch, while the cathode planes are at $\pm 45°$ with respect to the anode, and are wound with 50 μm wire on a 1 mm pitch. Both the cathode and the anode wires are read out to measure the electron coordinates.

On average, three photoelectrons are detected for each relativistic charged particle, and this enables a measurement of the radius of the Čerenkov circle ($\sim$ 70 mm) with an accuracy $\sim$ 0.7 mm, which in turn, allows good particle identification up to 200 GeV/c. See Fig. 5.

This device has been running routinely in the Fermilab experiment for the past three years.

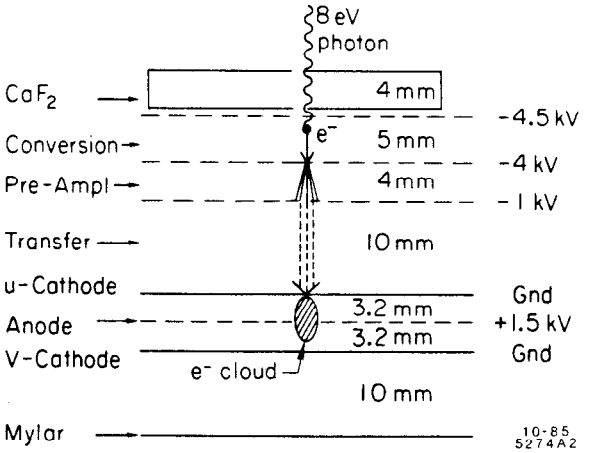

Fig. 4 A schematic of the grid structure in the photoelectron detector for experiment E-605 at Fermilab (Ref. 5).

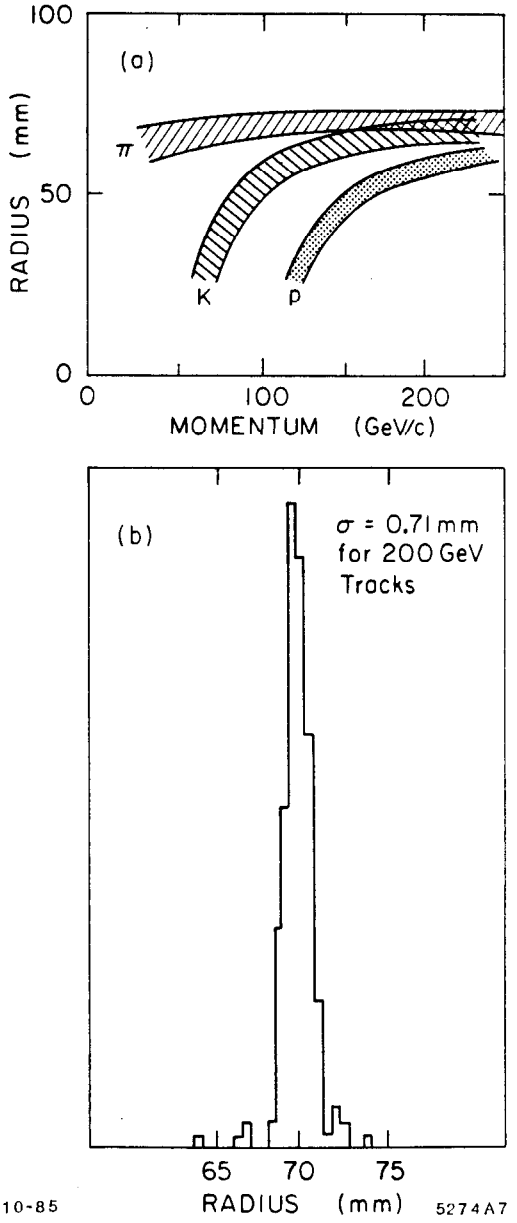

Fig. 5 (a) A schematic of the radius measurement for π, K, p as a function of momentum. (b) The measurement error for a sample of 200 GeV/c tracks.

2.2 Rutherford's RICH at the Omega Spectrometer

The Omega spectrometer is yet another multi-particle forward spectrometer experiment, this time in the high energy secondary hadron beam at the SPS at CERN. A layout of the spectrometer is shown in Fig. 6. This experiment is equipped with a large ring imaging Čerenkov counter[6] to provide final state hadron identification. It is designed to identify pions from (5-80) GeV/c and providing K/p discrimination up to 160 GeV/c. Dimensions of the Čerenkov counter are given in Fig. 7.

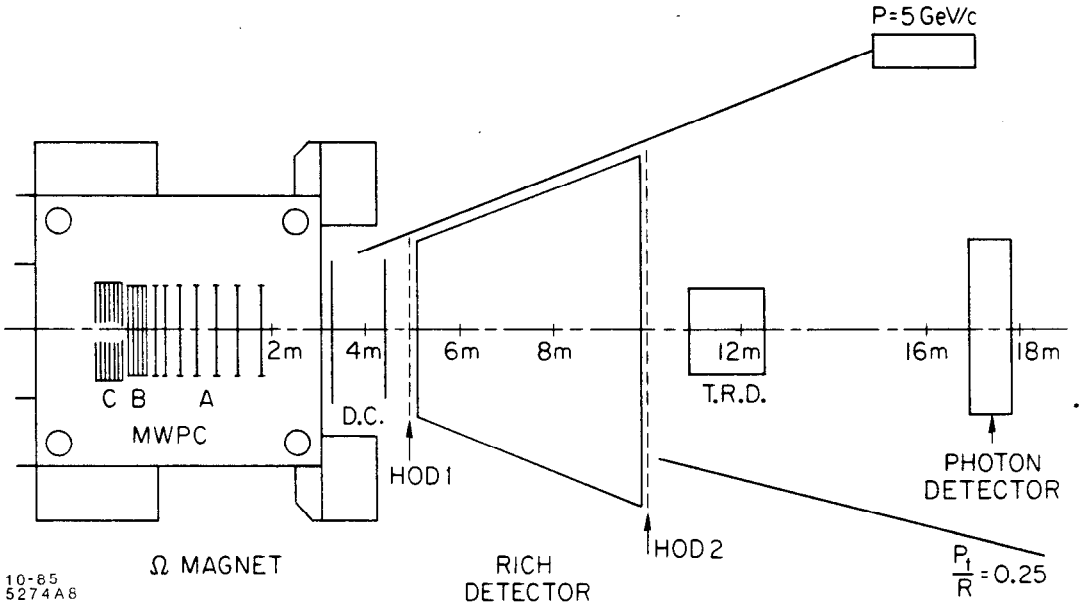

Fig. 6 A schematic of the Omega spectrometer experiment at CERN.

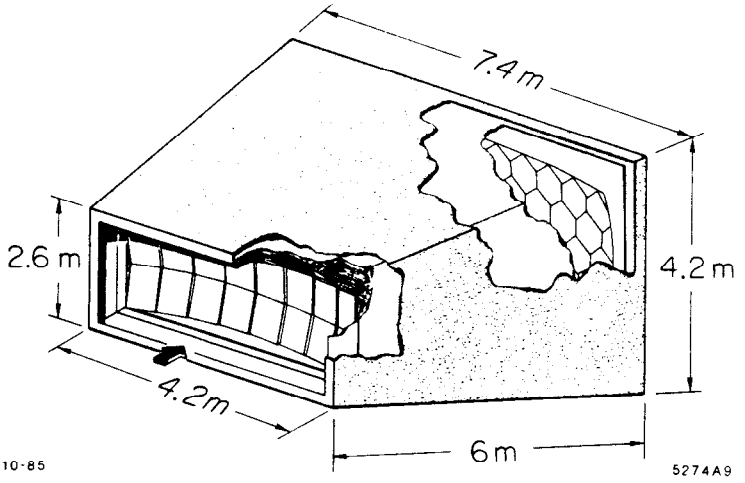

Fig. 7 A schematic of the ring imaging counter in the Omega Spectrometer at CERN. For details see Ref. 6.

The radiator is 5 meters of nitrogen gas. Čerenkov light from the radiator volume is focussed back onto the photon detectors, which are mounted at the focal plane of a 28 square meter spherical mirror array. The reflectance in the (170-250) nm region was measured to be > 75%. The Čerenkov light is detected in 16 TPC devices, each (40 × 80) cm^2 in area, and shown schematically in Fig. 8. The Čerenkov photons photoionize an organic vapor (Tetrakis Dimethylamino Ethylene – TMAE) which is added to the chamber gas mixture of methane/isobutane 80/20. The chamber gas is isolated from the radiator gas by the quartz windows shown in Fig. 8.

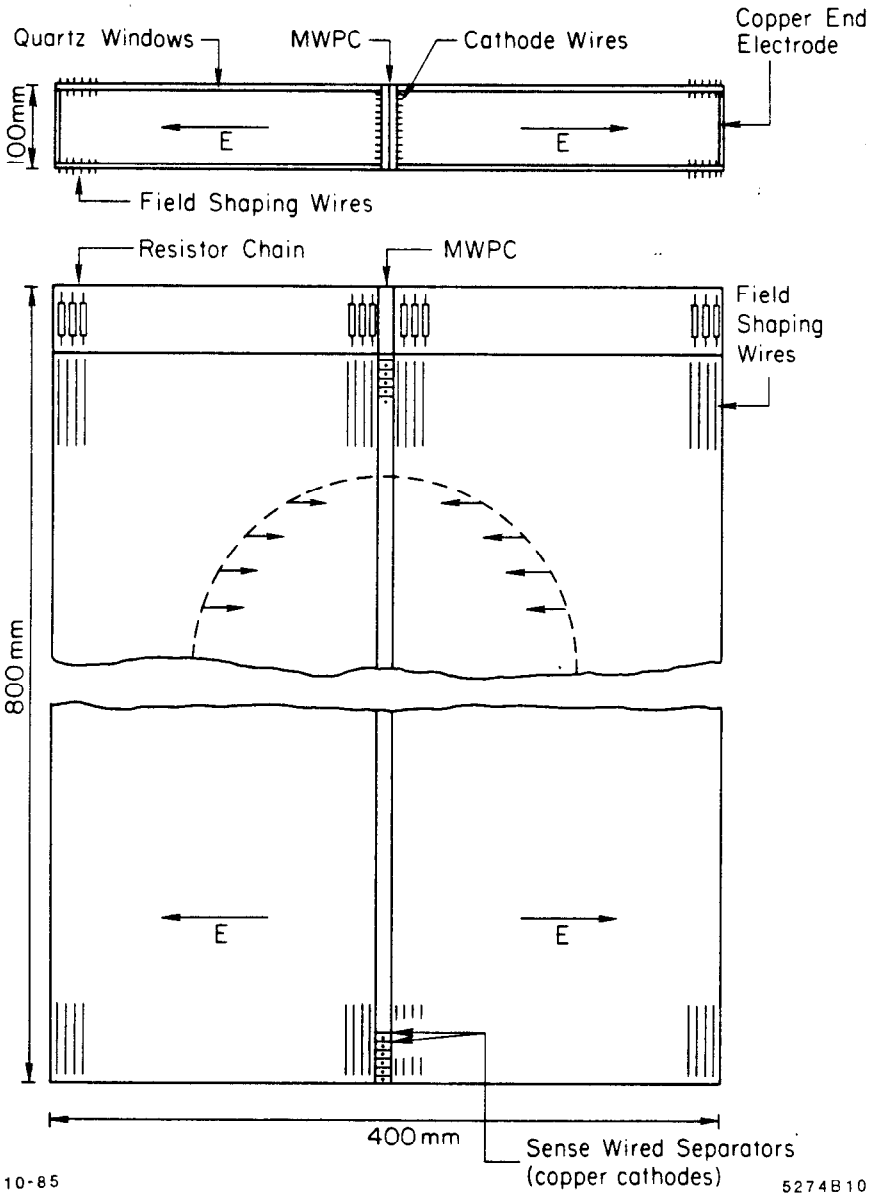

Fig. 8 A schematic of the photon detector for the Omega experiment at CERN.

Both windows and side walls of the TPCs are wound with an inner and outer field grid which establish a uniform electric drift field to transport photoelectrons from their creation point to the central MWPC detector. Measurement of the drift time and the wire address allows measurement of the Čerekov circle radius. (Note the intrinsic left-right ambiguity in this device).

The performance of this device is shown in Fig. 9. The accuracy of measurement of the Čerenkov ring radius is found to be $\sigma \sim 2.9$ mm, and allows good K/π identification up to nearly 80 GeV/c, and K/p identification up to about 160 GeV/c. The actual number of photoelectrons detected is about half than expected; they detect around 14 photoelectrons rather than the 28 calculated. The loss of photoelectrons is thought to be partly in the efficiency of detecting the single photoelectron and partly in the input electron optics to the MWPC shown in Fig. 8. This group is running again in the fall of this year with improved electronics and electron transport optics, and will also use a freon radiator gas. Improvements are expected from each of these changes. We wait, with great interest, their new results.

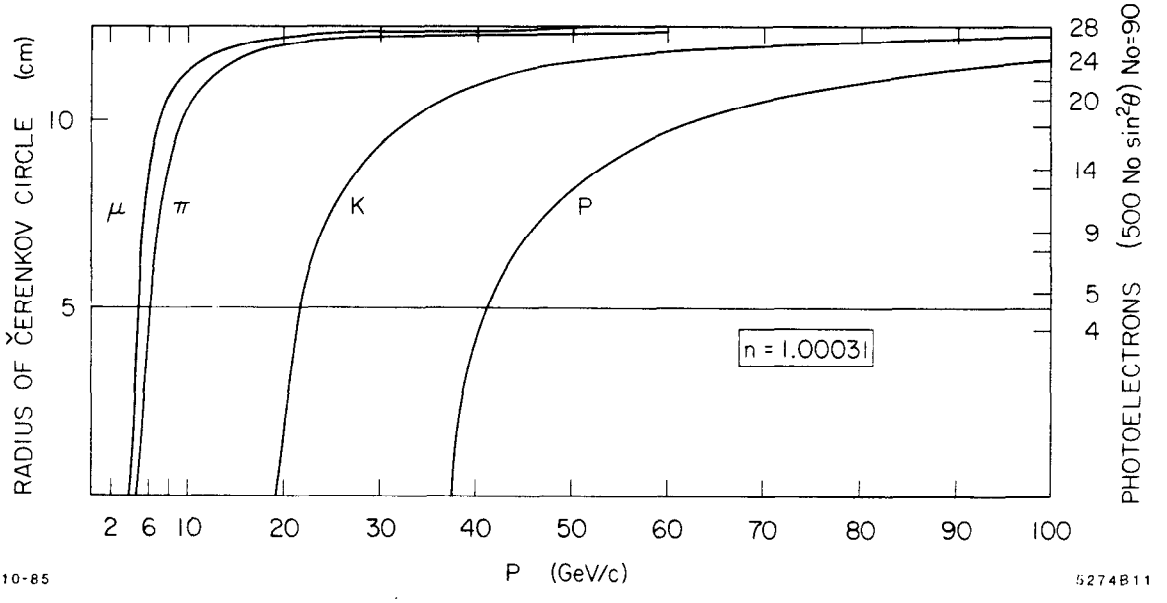

Fig. 9 The calculated performance of the Omega RICH.

2.3 The DELPHI Experiment at LEP and the SLD Experiment at SLAC

The DELPHI experiment is one of the four large experiments being built at CERN to study Z^0 production and decay at LEP. The usual quadrant view of the experiment is shown in Fig. 10, while the detail of the Ring Imaging Čerenkov Detector (RICH) is given in Fig. 11.

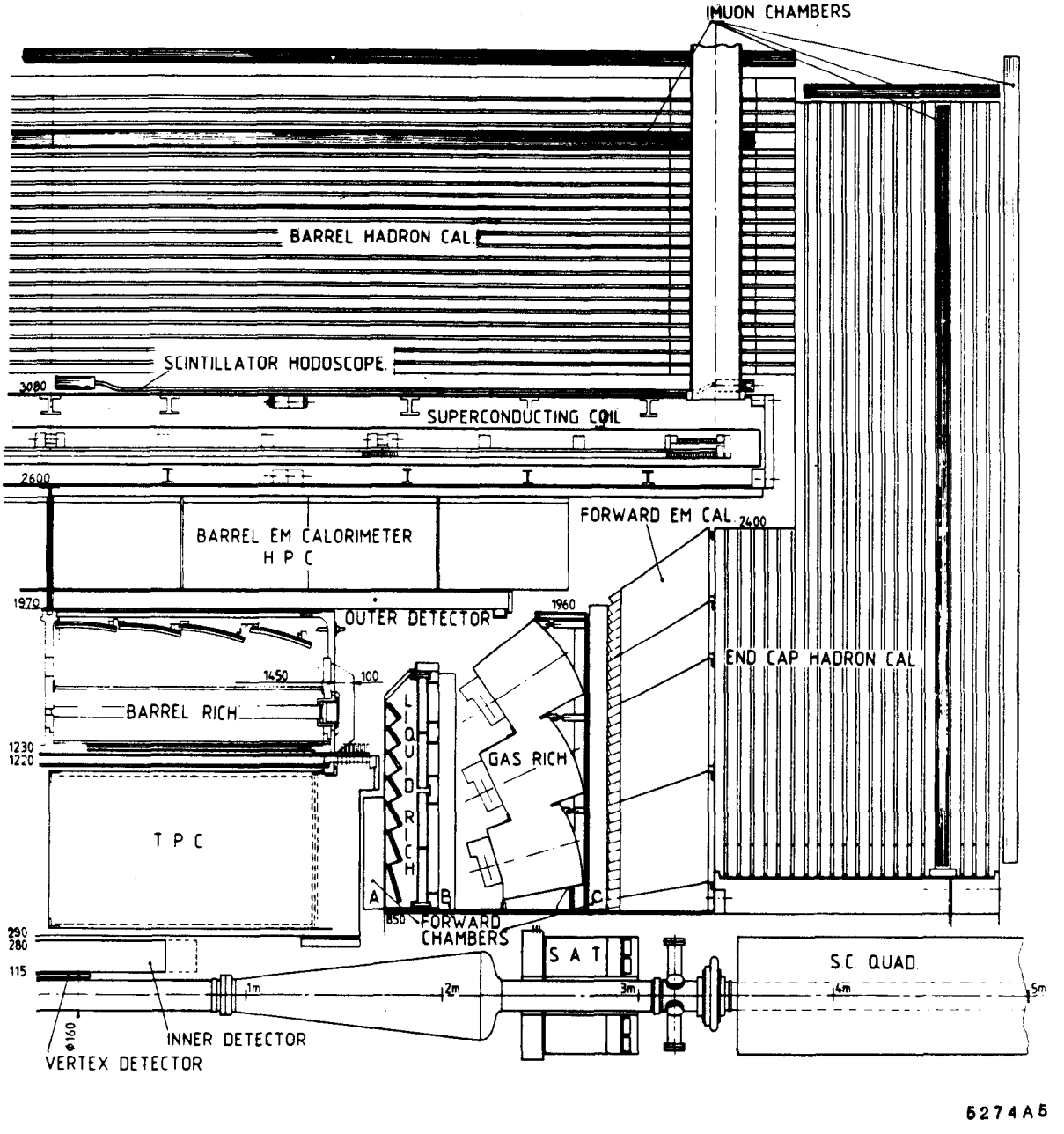

Fig. 10 General layout of the DELPHI experiment.

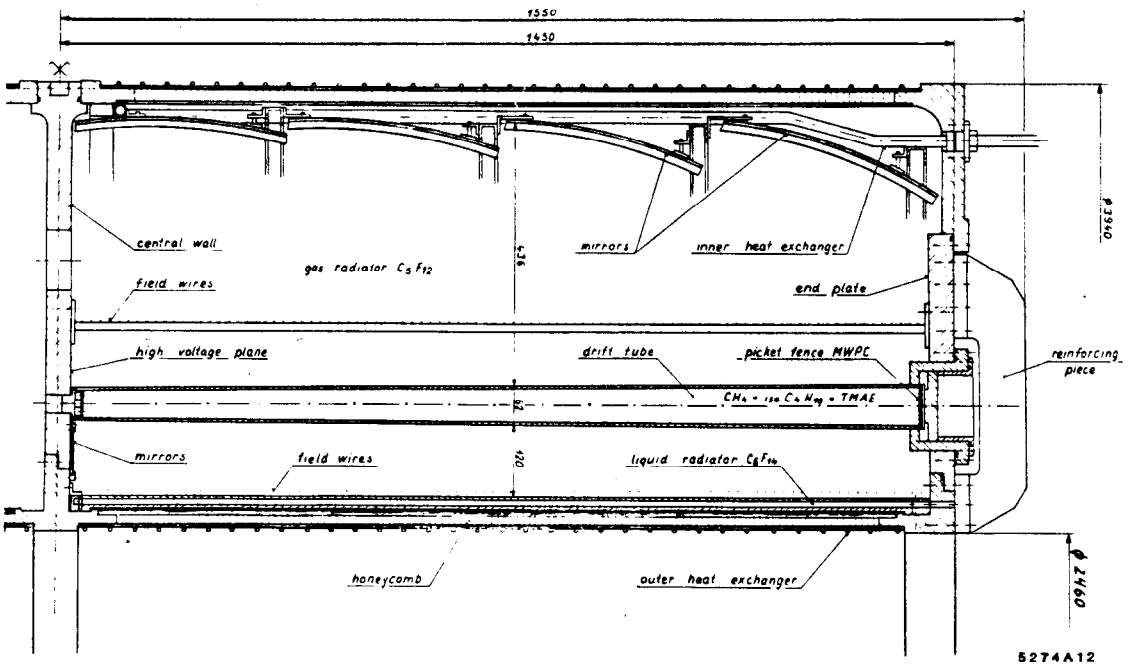

Fig. 11 Schematic of the RICH counter for the DELPHI experiment. For details see Ref. 7.

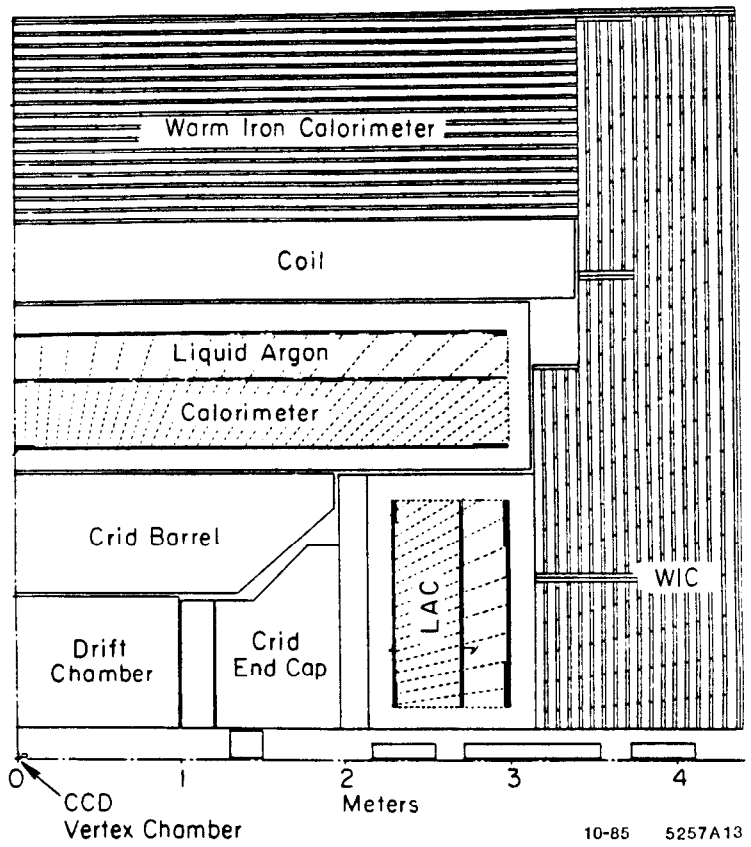

Fig. 12 General quadrant view of the SLD experiment.

The SLD experiment is the large new detector being built at SLAC to fully exploit the physics opportunities of the SLC. The usual quadrant view of this experiment is shown in Fig. 12, with the detail of the Čerenkov counter in Fig. 13.

Both DELPHI and the SLD devices use a double radiator scheme to provide an extended momentum range over which particle identification may be achieved. See for example Fig. 2. The principle is described below.

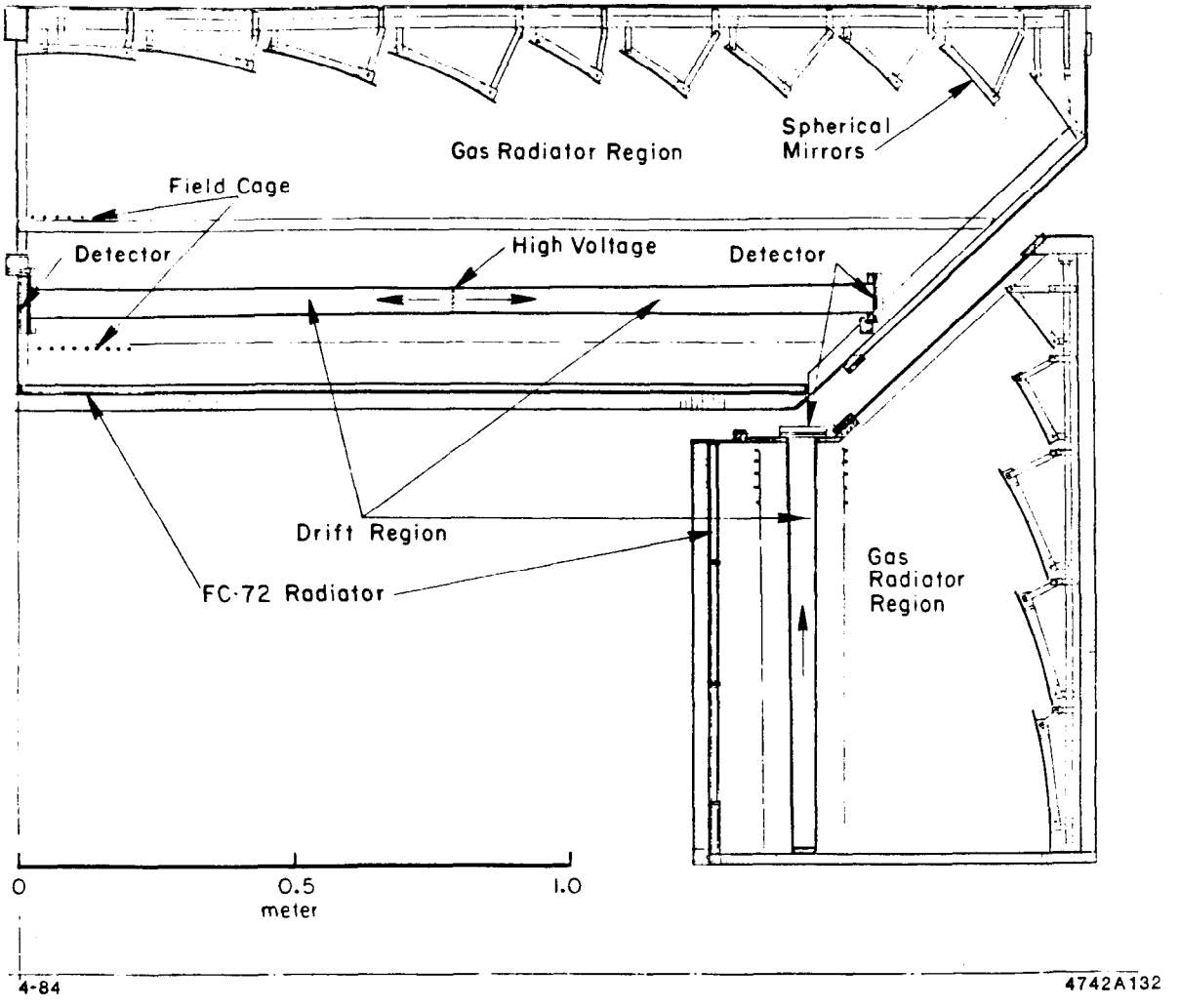

Fig. 13 Schematic of the CRID for the SLD experiment. For details see Ref. 4.

A relativistic charge particle passing through both radiators would generate patterns of light characterized in Fig. 14; the light from the liquid radiator, (C_5F_{12}), is proximity focussed on one side of the photon detector while the Čerenkov light from the gas radiator is focussed via spherical mirrors onto the other side of the photon detector. The image from the liquid is rather broad due to geometry and chromatic effects, and has a radius of about 17 cms. It is expected to have about 24 photoelectrons distributed around its circumference. The image from the gas radiator (isobutane or C_6F_{14}) should be about 3 cm radius, be rather sharp and have about 12 photoelectrons.

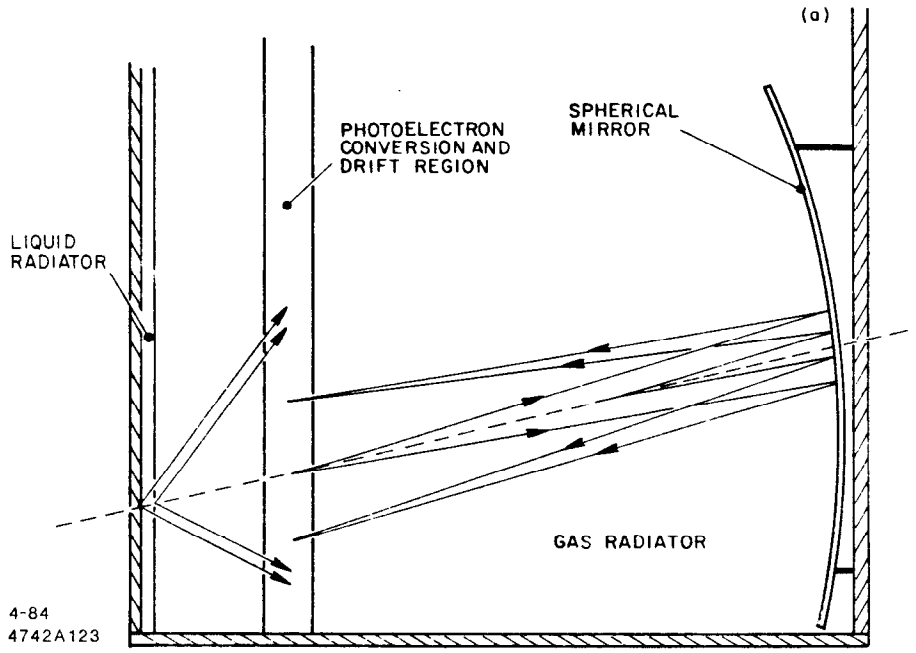

Fig. 14 A schematic representation of the two radiator geometry used in the Čerenkov ring imaging detectors in DELPHI and SLD.

The photon detector is a double-sided quartz box (to transmit the Čerenkov light) with a double electric field cage wound on the inner and outer walls of the box to create an uniform electric drift field along the axis of the box. See Fig. 15. The photons are detected by photoionization of Tetrakis Dymethyl Amino Ethylene (TMAE), which is present at 0.1% level in a 70 : 30 methane : isobutane gas mixture. The TMAE has a very high photoionization cross section in the (1700-2400) Å region, and so acts as a very efficient photocathode. Photoelectrons will drift under the action of the parallel electron and magnetic fields to a multi-wire proportional chamber detector. The drift time and wire address provide two of the coordinates of the creation point of the photoelectron. Information on the depth at which the photoionization took place is found from localization of the avalanche along the wire.

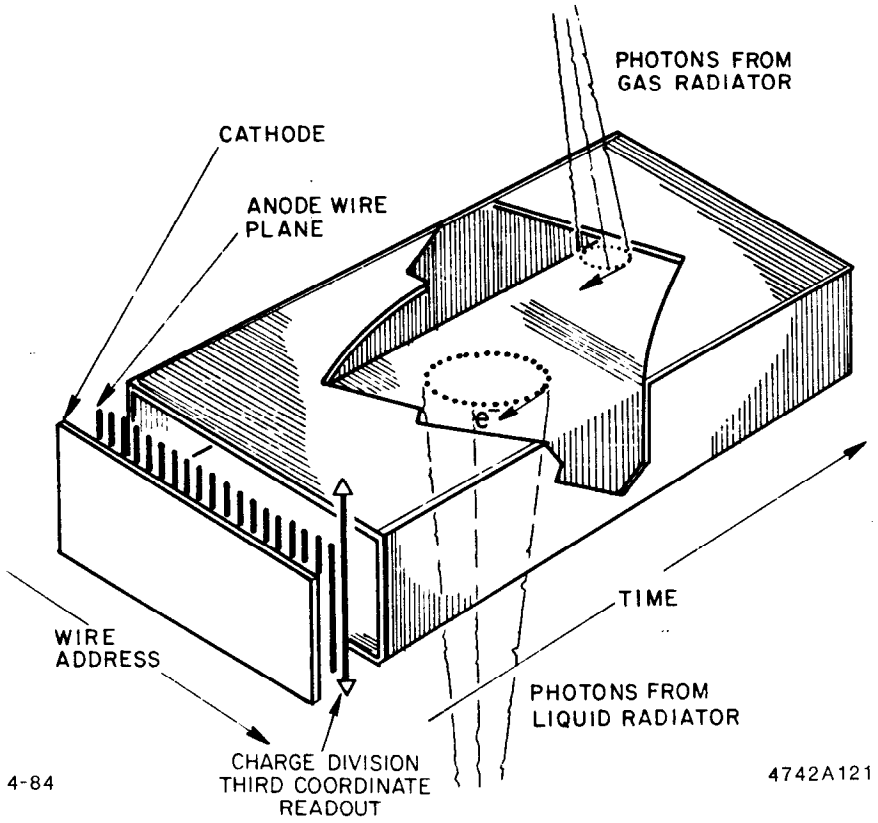

Fig. 15 Schematic of the photon detector boxes used in DELPHI and SLD.

The Delphi and SLD devices have rather similar specifications. As an example of these systems, a summary of the parameters of the SLD device is given below in Table I.

A demonstration of the power of the full particle identification system in SLD, (*i.e.*, vertex detector plus CRID) is shown in Fig. 16. A Monte Carlo study of Z^0 decays within the SLD detector has been performed.[8] The charmed meson decay of the heavy boson was chosen as typical of the heavy quark decays and the $D \rightarrow \mathrm{K}\pi\pi$ decay of the D as used to study the performance of the detector. The $(\mathrm{K}\pi\pi)$ mass distribution is plotted in Fig. 16 for four separate selections of data; (a) displays the $\mathrm{K}\pi\pi$ mass for all appropriately charged three-track combinations which belong to the same jet–very little sign of the D-meson is observed. (b) shows $\mathrm{K}\pi\pi$ combinations that have been identified by the CRID; a clear D-meson peak is observed with a signal-to-noise of about 1 : 3. (c) displays the $\mathrm{K}\pi\pi$ mass for unidentified tracks coming from a secondary vertex as measured by the high resolution CCD vertex detector in SLD; a very clear D peak is seen with a signal-to-noise of about 3 : 1. And finally in (d) the $\mathrm{K}\pi\pi$ mass spectrum is plotted for identified π's and K's, that come from a separated, secondary vertex; an extremely clear D signal is observed with rather good tagging efficiency, $(\epsilon \sim 35\%)$.

This ability to clearly and efficiently tag heavy quark decays (t, b, c), of the Z^0 should enable studies of very small branching ratio decays into heavy flavor mesons, allow detailed study of the cascade process $t \to b \to b \to c \to s$, and of $B - \bar{B}$ and $D - \bar{D}$ mixing.

Table I

Summary of Parameters of the SLD CRID

	Liquid	Gas
Solid Angle	98%	94%
Angular Acceptance: Endcap	$10.5° - 37°$	$8.5° - 33°$
Barrel	$37° - 90°$	$38° - 90°$
Radiator	FC-72	Isobutane
Index of Refraction (6.5 eV)	1.277	1.0017
Focusing	Proximity	Spherical mirror
Č Threshold (γ)	1.61	17.5
Č Ring Radius	17 cm	2.8 cm
N_{pe}	23	13
P_{thresh} (3 p.e.)		
e	$\sim$ 1 MeV/c	$\sim$ 10 MeV/c
π	0.23 GeV/c	2.6 GeV/c
k	0.80 GeV/c	9.5 GeV/c
p	1.50 GeV/c	17.8 GeV/c

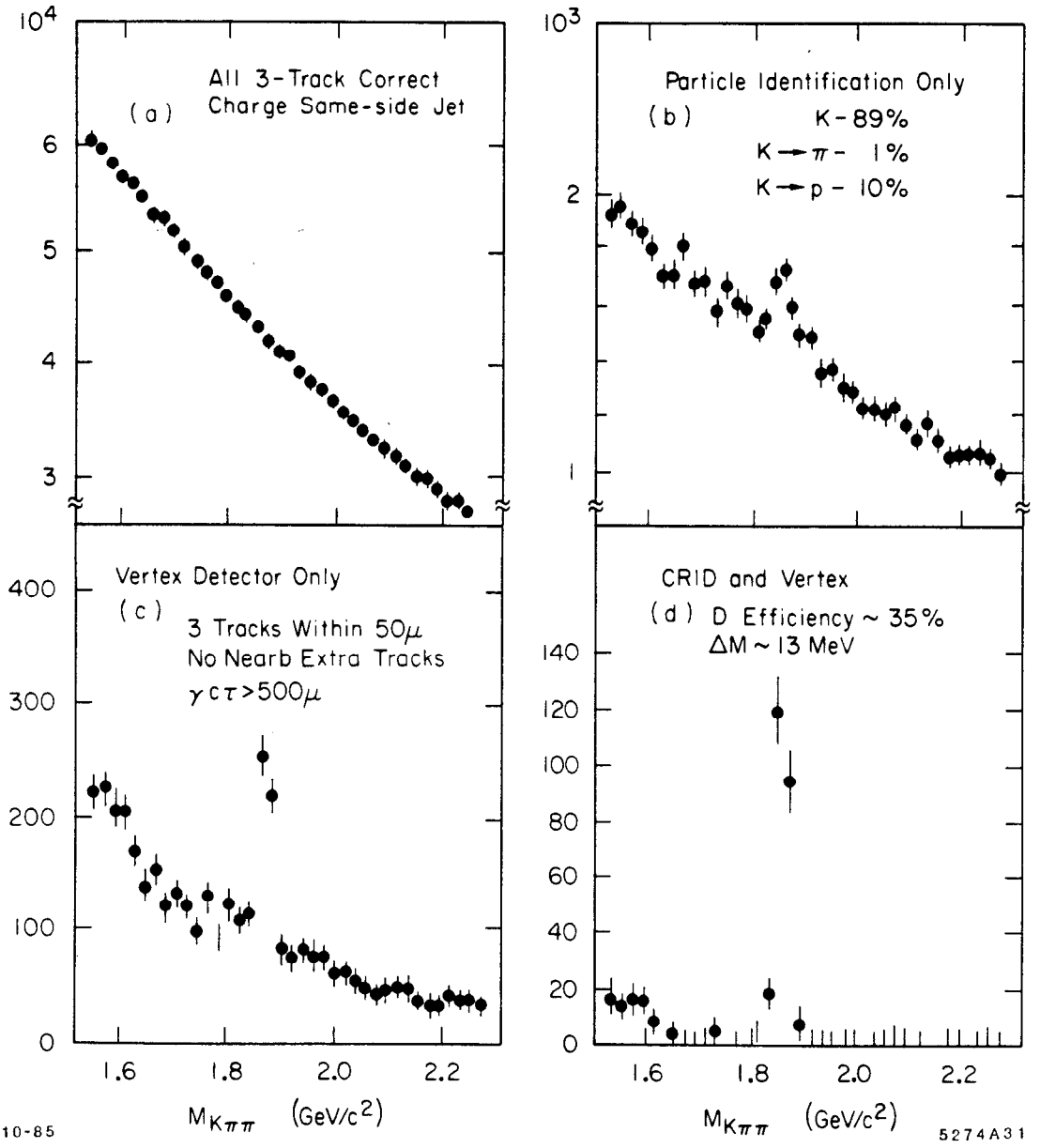

Fig. 16 Mass distribution of $K\pi\pi$ combination resulting from Z^0 decays. (a) All appropriately charged combinations. (b) Identified π and K candidates using the CRID. (c) Three appropriate charged particles coming from a secondary vertex. (d) Identified π's and K's which come from a separated secondary vertex.

3. R&D STATUS OF THE NEW 4π DETECTORS

There are two 4π ring imaging detectors currently under development. The SLD CRID being built at SLAC, and the DELPHI RICH detector being built at CERN. The R&D progress for both detectors is described below.

3.1 SLD R&D Progress

The SLD CRID group has been working on a 'proof-of-principle' prototype, designed to test most of the detector ideas in a full scale device, but not in the specific geometry or the actual construction techniques used in SLD. The device is shown schematically in Fig. 17.

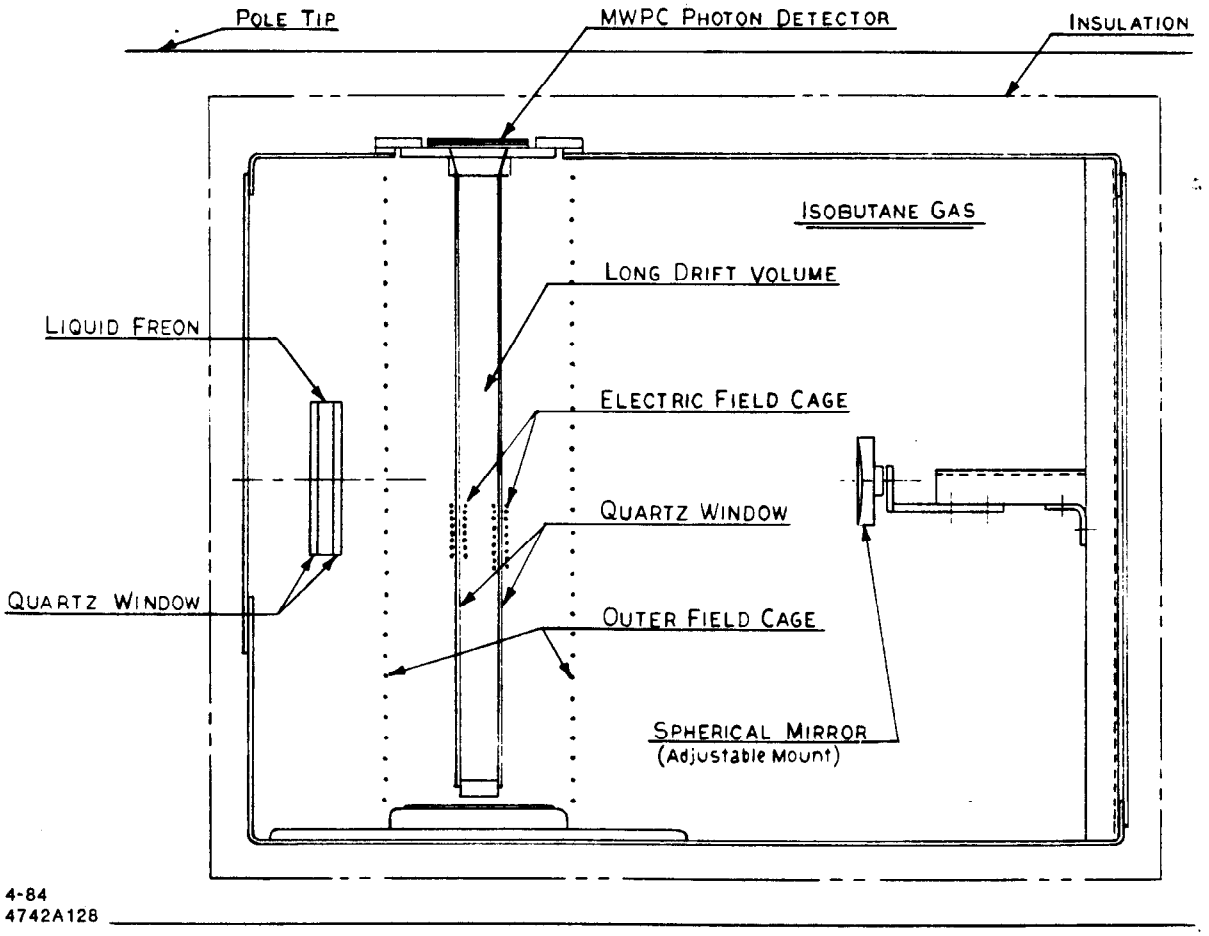

Fig. 17 Schematic of the "proof-of-principle" prototype of the CRID under test at SLAC.

The prototype elements are mounted within an aluminium box, 1 meter on each side, which can be inserted between the pole tips of a large electro-magnet providing fields up to 18 kG. The test devices were:

- a liquid radiator cell, which is an all quartz cell 1.27 cms thick and connected to an external pump to circulate C_6F_{14}, perfluorohexane radiator liquid through external oxysorb filters to remove oxygen and water vapor.
- a secondary electrostatic field cage, wound with 1 mm diameter copper wire on a 2.5 cm pitch. This cage helped maintain electric field uniformity in the photon detector box, and isolate it from the nearby electrical grounds.
- the photon detector box, which is a quartz box with a double window of dimension 20 × 80 cms, 4 cms deep at one end, increasing to 6 cms depth at the detector end. A double field cage is wound on the inner and the outer surfaces of the detector box, with a 2.5 mm pitch, providing an adjustable electric field in the range (50-650) v/cm. The box is filled with a gas mixture – (CH_4 (70%), isobutane (30%), TMAE ($\sim$ 0.1%) – which was circulated at flow rates of (5-40) ℓ/hr. The TMAE acts as the photocathode.
- a spherical mirror, with good ultraviolet reflectance, ($\gtrsim$ 86% in the region (1700 - 2400 Å), and adjustable so that it could image the Čerenkov light produced in the 43 cms of gas radiator back onto the photon detector box at any desired position along the length of the box.
- an electron detector, to efficiently detect the single photoelectrons released from the TMAE. The electrons are detected by a picket fence of multiwire proportional counters working at a gas gain of between 1 and 2 $\times 10^5$. In order to avoid a positive feedback situation one has to limit the illumination of the TMAE volume by the light emitted in the avalanche at the anodes of the MWPCs. This protection from photon feedback is achieved by mechanically limiting the solid angle and is discussed below under detector development.

The prototype was installed in a momentum analyzed secondary beam which could deliver either electrons or hadrons to the experiment. The response of the device to 11 GeV/c hadrons is shown in Fig. 18(a), a two-dimensional plot of time versus wire address integrated over 200 beam tracks. The plot shows the gas ring, the front and rear sectors of the liquid ring and the beam spot. Fig. 18(b) shows the gas ring by itself. The width of the gas ring is dominated by the parallax error from the lack of information on the third (depth) coordinate.

Figure 19 shows a single event display; (a) for the full event and (b) for the gas ring only. The solid lines are fiducial regions for the gas and liquid rings.

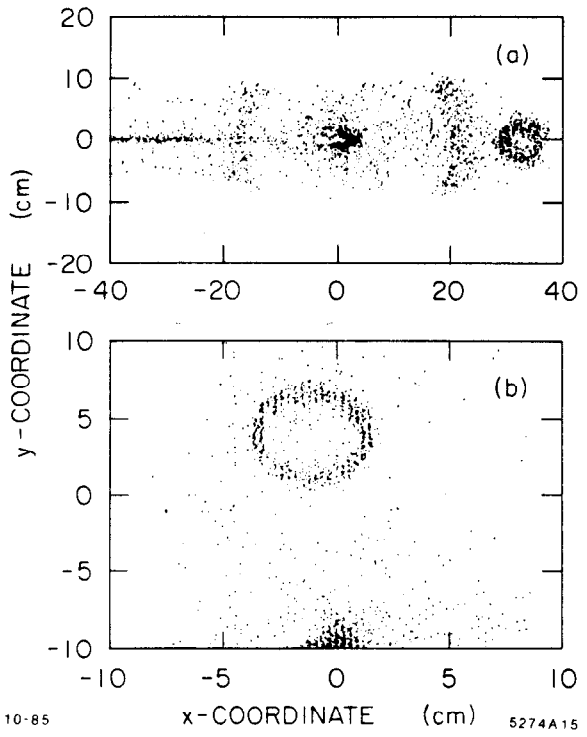

Fig. 18 (a) On-line residual plot of 200 beam tracks; y is the wire address and x is derived from the drift time. (b) A similar plot on an expanded scale showing the gas ring alone.

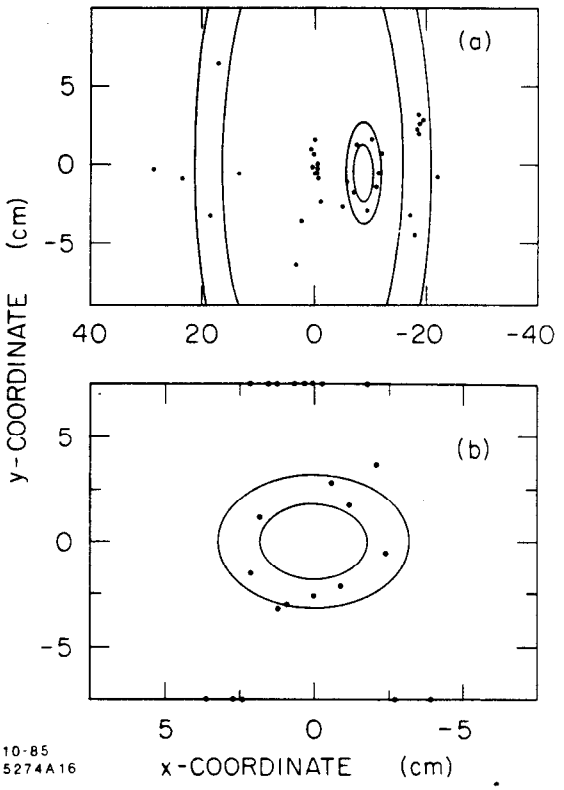

Fig. 19 Single event display of wire address against drift time.

Fig. 20 is the radius plot for the gas ring, and shows good signal-to-noise with very little background. The number of detected photoelectrons for each gas ring is shown in Fig. 21, and compared to a poisson distribution for $\bar{n} = 7$.

The number of photoelectrons detected from the liquid radiator is shown in Fig. 22, where the bottom scale is the actual number found for the leading sector of the ring, and the upper scale is the number of photoelectrons calculated for the full ring circumference. About $\sim$ 18 photoelectrons per particle are detected from the liquid radiator.

It is clear from the difference in populations of the leading and trailing sectors of the liquid ring in Fig. 18(a), that electrons are being lost as they drift down the photon detector box. We measured the attenuation lengths quantitatively by: i) varying the drift velocity (and therefore the drift time), of the photoelectron by changing the drift field, and ii) by changing the position of the focus of the gas ring by adjusting the mirror orientation. Both methods yield an electron attenuation length of approximately 35 cms (see Fig. 23). An average

of 13 photoelectrons per incident particle for the gas radiator, and an average of $\sim$ 37 photoelectrons per incident particle for 1 cm of liquid radiator were observed after correcting for the electron attenuation length. These yields exceed our expectations.

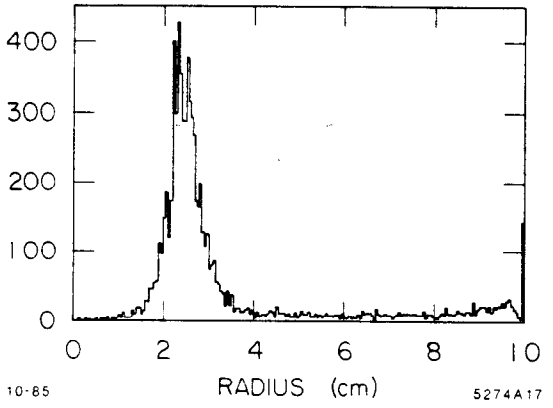

Fig. 20 The radius of the Čerenkov ring for light from the gas radiator. The width of this distribution agrees well with the Monte Carlo calculations for measurements excluding the depth information.

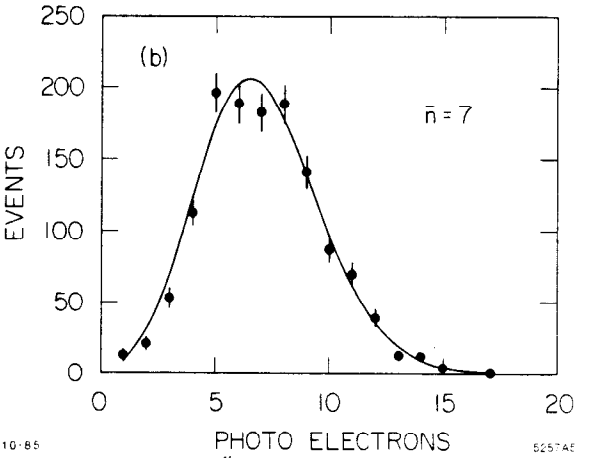

Fig. 21 The number of photoelectrons detected per event for the Čerenkov ring produced by the gas radiator.

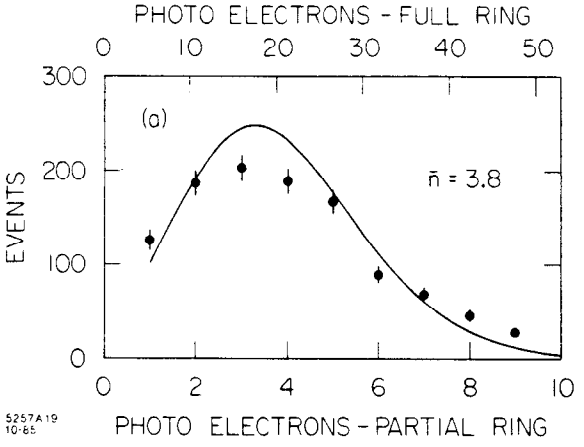

Fig. 22 The number of photoelectrons detected per event for the leading arc of the Čerenkov ring produced by the liquid radiator. The upper scale gives the scaled number that would be detected for the full ring.

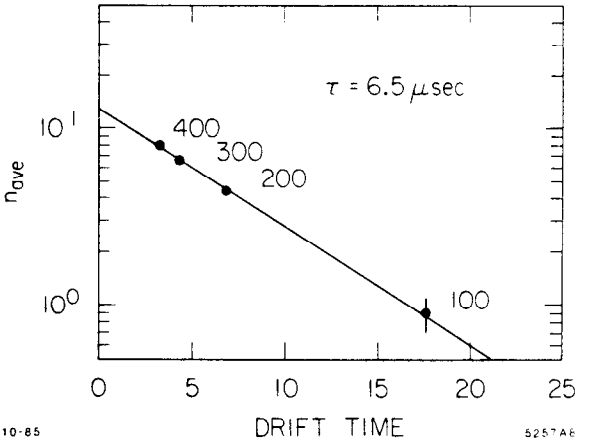

Fig. 23 The average electron "lifetime", or attenuation length, derived from the number of electrons on a gas ring versus the electron drift time. The drift time is determined by the electric drift field which is shown in the figure in volts/cm.

The device was tested with incident pions from 4 GeV/c to 11 GeV/c. Fig. 24 displays the Čerenkov angle measurements from the CRID prototype.

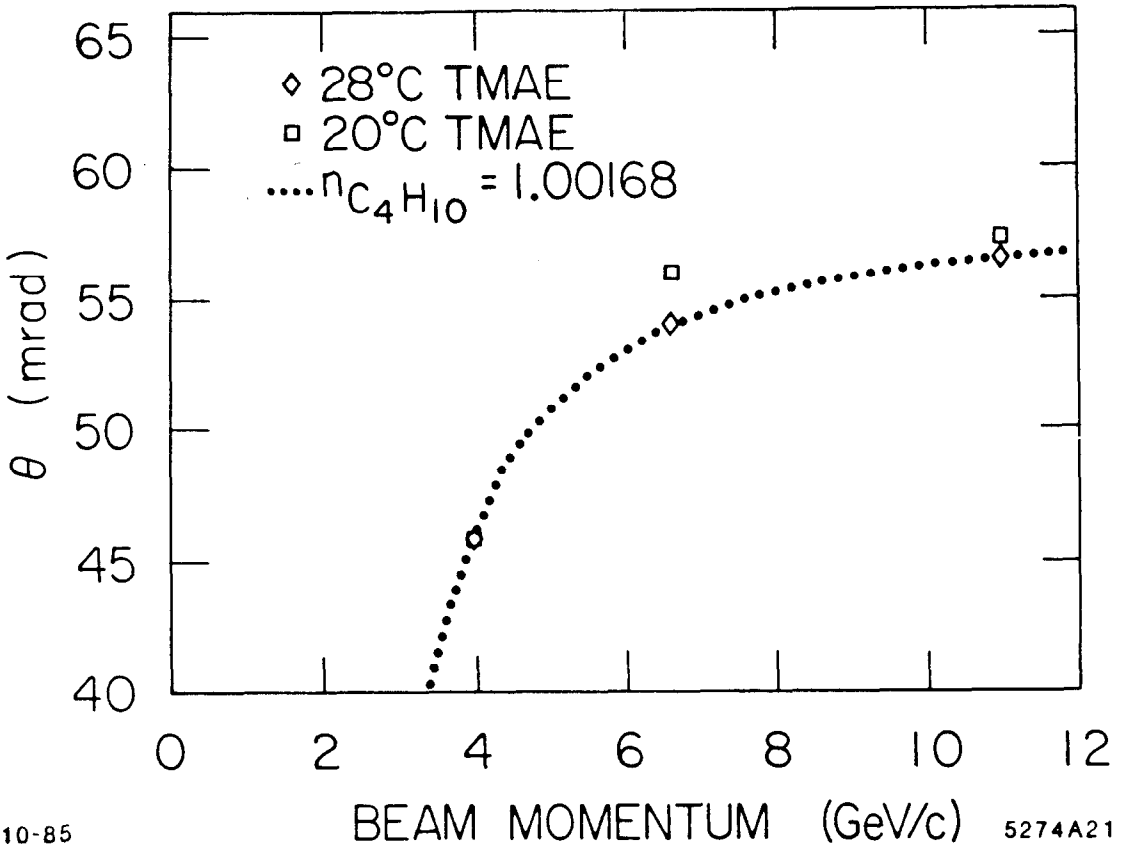

Fig. 24 The dependence of the measured Čerenkov angle for tagged pions as a function of momentum.

At 4 GeV/c, the beam was tuned to deliver a mixture of electrons and pions, the beam particle being tagged by a threshold Čerenkov counter. Fig. 25 shows single event displays for a) an electron and b) a pion incident on the CRID prototype. The dotted circles indicate the expected Čerenkov circles for pions (inner) and electrons (outer), while the crosses are the detected photoelectron coordinates. The solid line is a fit to the data.

Fig. 26 shows the distributions of the Čerenkov angles for the tagged pion and electron samples, as measured by the CRID prototype. A clear 3 σ separation is observed even without third coordinate (depth) measurement. It is interesting to note that a factor of four reductions of the width of these distributions is expected when the third coordinate information is available.

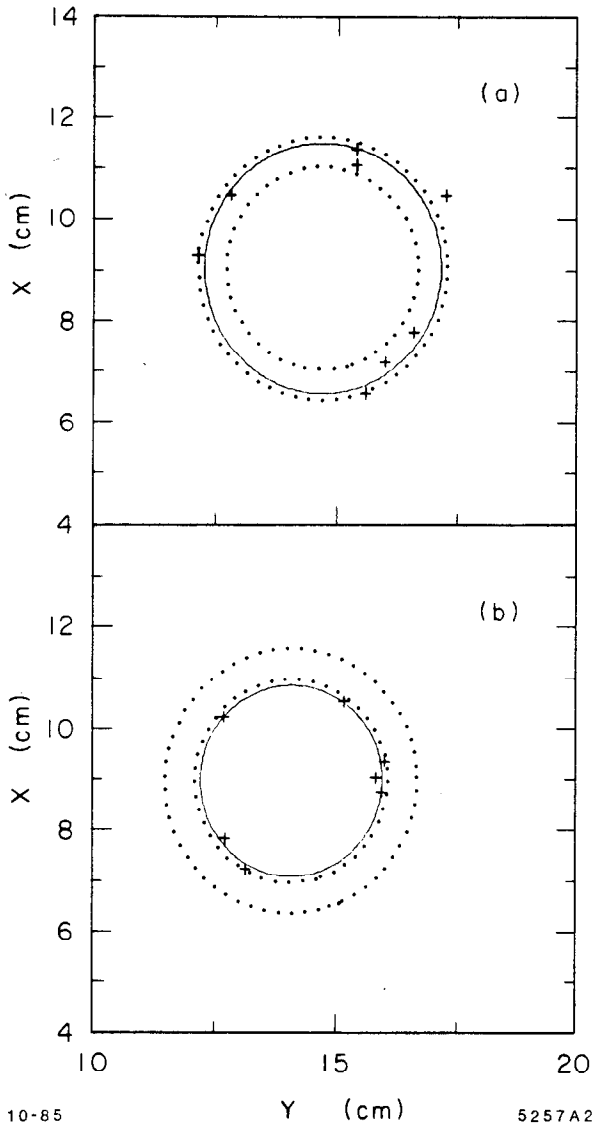

Fig. 25 The Čerenkov circles for single events with a) an electron, and b) a pion incident.

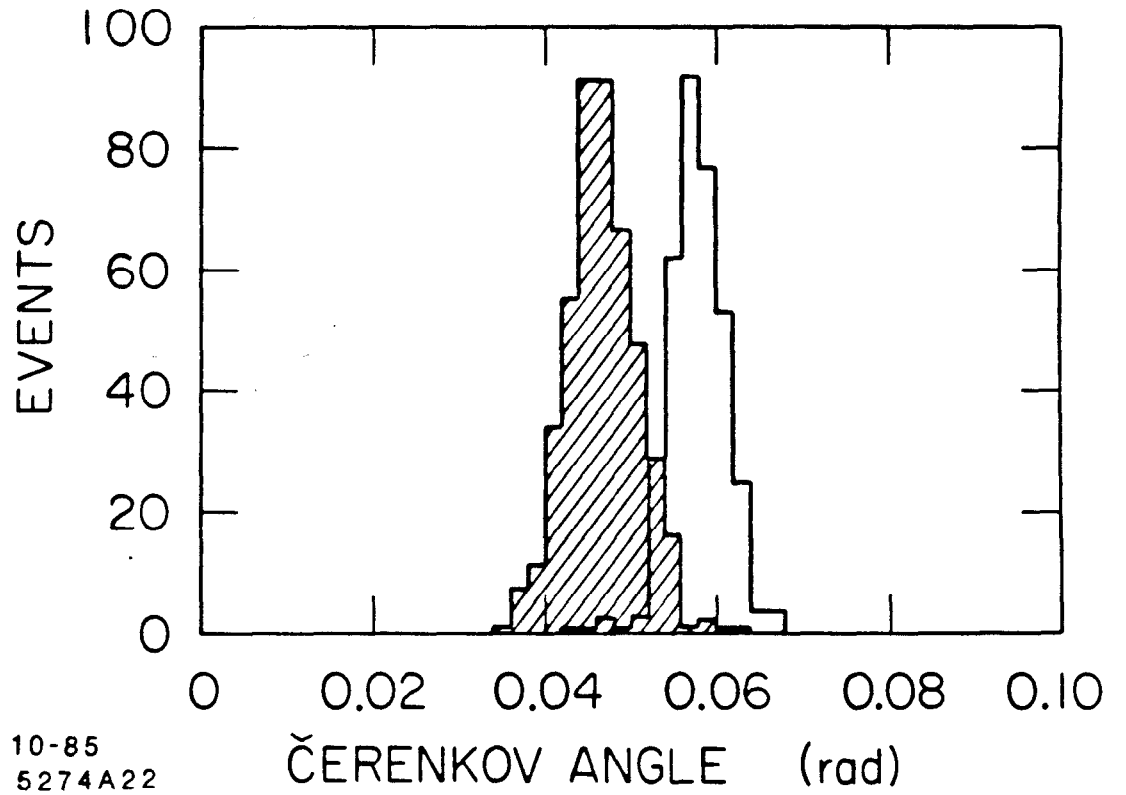

Fig. 26 The distribution of measured Čerenkov angles for tagged 4 GeV/c electron and pion incident on the SLD CRID prototype.

3.2 SLD Detector Development

The requirements for the CRID electron detector are:

— good single electron detection efficiency,

— efficient input optics from the drift region,

— protection against photon feedback,

— unaffected by $E \times B$ force.

The data discussed above was taken with the electrostatic structure shown in Fig. 27. Protection against photon feedback is achieved by the geometrical shielding of the TMAE drift volume by an array of thick wires; this reduces the feedback noise by a factor of four to five. The input optics efficiency is calculated to be essentially 100% and laser scanning measurements corroborate this value.

The main unanswered question in the detector design is how to obtain the third coordinate (depth) information.

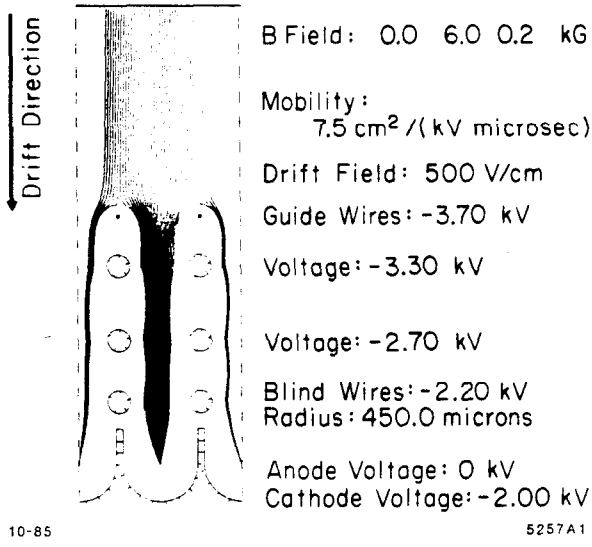

Fig. 27 An electrostatic simulation of the detector electron collection efficiency with a four layer 'blinding grid.' A 6 kG axial magnetic field with a 200 gauss radial component is assumed in the calculation. Data discussed in the text were taken with no magnetic fields.

This measurement dominates the accuracy of the angular resolution of the CRID. A variety of techniques can be employed to make this measurement (*e.g.*, cathode strips, wedge cathode, graded cathode, resistive cathode or resistive anode). The technique of choice should provide (i) resolution of order 1 mm, (ii) good solid angle coverage and (iii) good channel-to-channel signal isolation. Good progress has been made in implementing a resistive anode readout employing charge division on short ($\sim$ 5 cms) wires, to provide the third coordinate information.

Fig. 28 shows the charge ratio measured in a single cell test chamber constructed with a 7 μm diameter carbon filament as the anode, and read out with two low noise HQV810 preamplifiers measuring the charge at opposite ends of the fiber. These results indicate a position measurement of better than 2% accuracy of the total length. This corresponds to a resolution $\sigma \sim 1$ mm for the depth measurement, and is found to be uniform along the length of the fiber.

We have constructed a chamber with 60 carbon fiber anodes, in the geometry shown in Fig. 27 above, and collected data with pions and electrons. The analysis of the Čerenkov rings data is currently on progress, but should be reported at the IEEE meeting in San Francisco in October 1985.

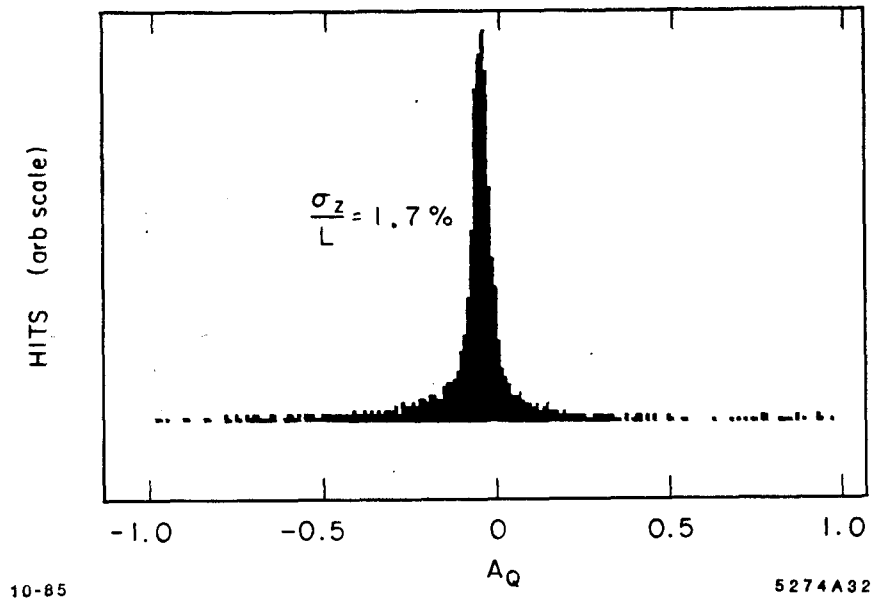

Fig. 28 Charge division measurement.

3.3 DELPHI R& D Progress

The DELPHI experiment at LEP has an aggressive and comprehensive prototype and development program for their RICH work. They have successfully passed the CERN Program Committee milestones for demonstration of the RICH subsystem and are proceeding with the design and construction of the final RICH modules.

Figure 29 shows a perspective of the DELPHI RICH prototype. The liquid radiator is C_6F_{14}, 1 cm thick, and the gas radiator is 47 cm of isobutane. The drift tubes were filled with a gas mixture of 95/5 methane/isobutane, with about 0.1% of TMAE as the photoionizing agent. Čerenkov light from single liquid radiator cell illuminates three drift boxes of 1 m 50 cm length, read out at one end by a MWPC. A uniform drift field is created by an inner and outer field cage wound on each drift box. A secondary field cage isolates the nearby electrical grounds in the prototype geometry. Light from the gas radiator volume is focused back on the top side of the drift tubes by three parabolic mirrors.

The response of this prototype to a 10 GeV/c hadron beam is shown in Figs. 30(a) and (b), two-dimensional plots of the drift time and wire address information. Fig. 30 (a) shows the liquid ring spread over three drift tubes, while Fig. 30 (b) shows both the liquid and the gas ring. Fig. 31 shows single event plots with the same information.

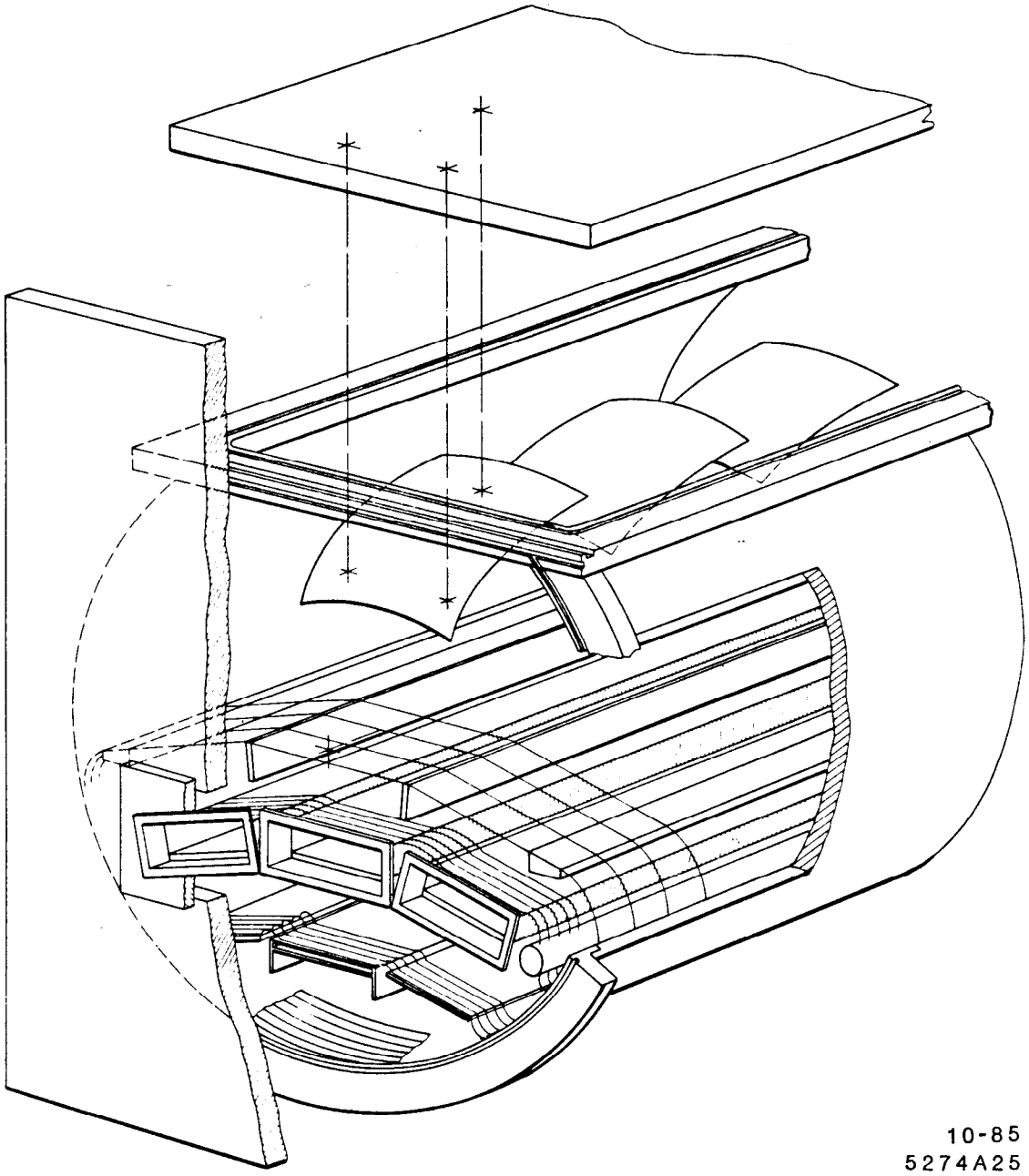

10-85
5274A25

Fig. 29 Schematic of the DELPHI RICH prototype.

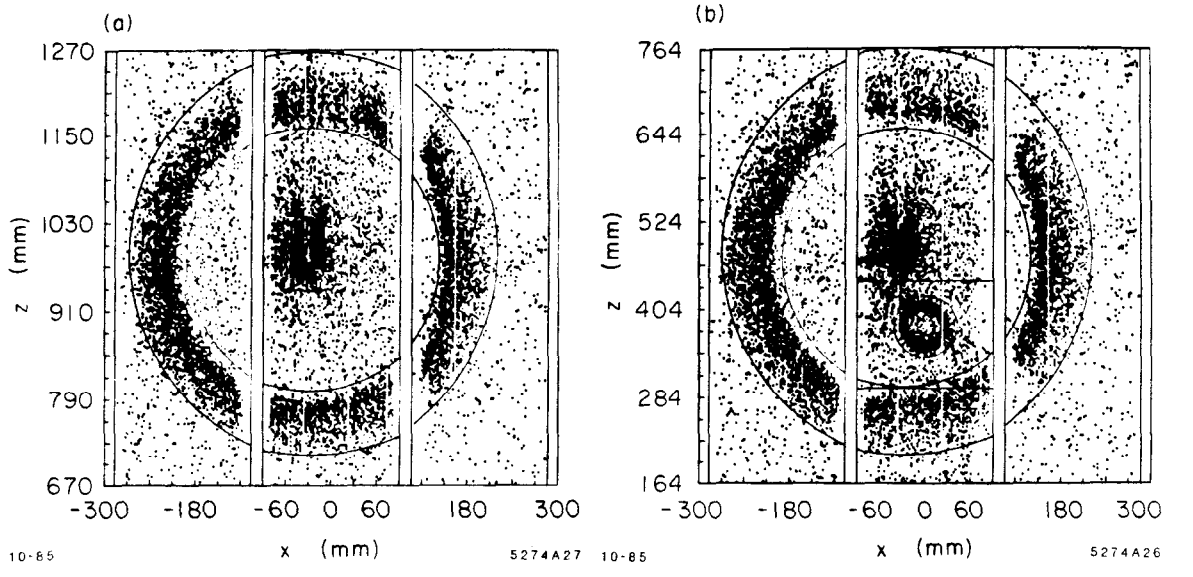

Fig. 30 Two dimensional plot of the photoelectron positions from the DELPHI prototype. The x–coordinate is the wire address and the z–coordinate is the drift time. The plot is an accumulation over several hundred beam tracks: (a) shows the liquid ring, (b) displays both the liquid and the gas rings.

Fig. 32 shows the radius plot for the liquid and the gas rings. Fig. 33 indicates $\sim$ 5.5 photoelectrons detected from the gas radiator and $\sim$ 17 photoelectrons detected from the liquid radiator. Their best results from recent beam tests have achieved $\sim$ 8.5 photoelectrons from gas and $\sim$ 19 photoelectrons from the liquid radiators respectively. When corrected for electron attenuation and drift losses, these results imply $\sim$ 12.7 photoelectrons produced in the gas ring, and $\sim$ 22.7 photoelectrons produced in the liquid ring, in very good agreement with their expectations.

The accuracy of measuring the Čerenkov ring is shown in Fig. 34 for both gas and liquid radiators. The gas and liquid rings are measured to have a radius of 27.8 $\pm$ 1.5 mm and 209.6 $\pm$ 5.5 mm respectively. Both measurements are made without the third coordinate information and achieve the accuracy predicted from the Monte Carlo simulation.

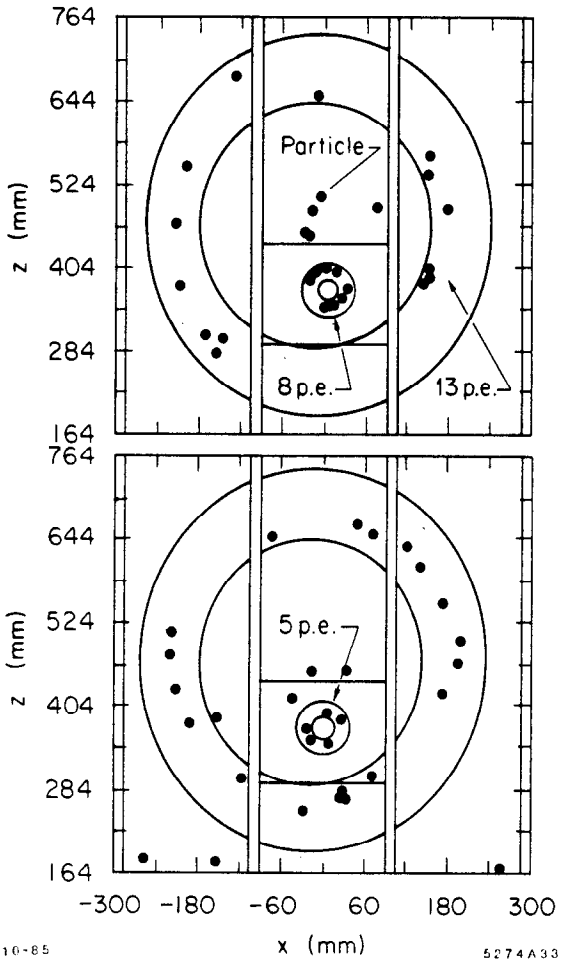

Fig. 31 Single event plots of wire address versus drift time.

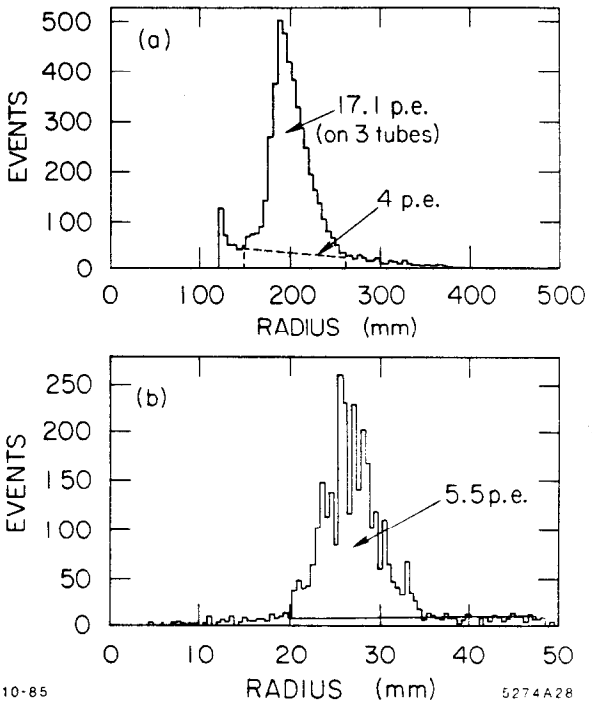

Fig. 32 The distribution of photoelectron hits as a function of the radius from (a) the gas ring, and (b) the liquid ring.

The DELPHI group observed quite long attenuation lengths for drifting electrons in the methane/isobutane gas mixture ($\sim$ 2-5 m), in contrast to the experience at SLAC ($\sim$ 0.3 m). Additional experiments with ethane/methane mixtures instead of isobutane/methane results in even longer attenuation lengths, ($\gtrsim$ 15 meters). Further studies of electron attenuation lengths with different gas mixtures, and chemical studies of these gas mixtures are being pursued by both the CERN and SLAC groups.

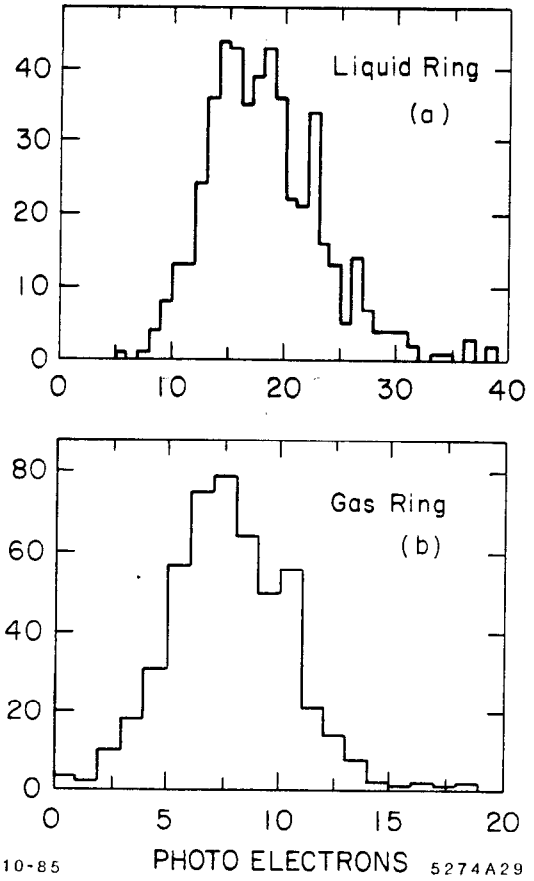

Fig. 33 The number of photoelectrons observed from the (a) liquid ring, and (b) the gas ring, in the DELPHI prototype.

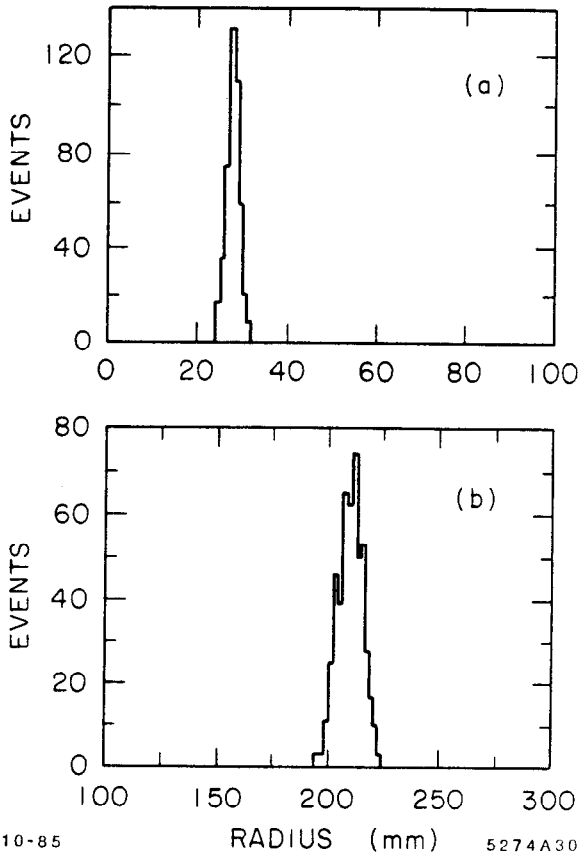

Fig. 34 The distribution of corrected radius measurements for the gas ring and liquid ring, from the DELPHI prototype.

4. SUMMARY AND CONCLUSIONS

4.1 Progress in the 'Problem Areas'

At the beginning of this review, I listed a number of problem areas, where progress had to be made before one could proceed to construct large ring imaging systems. Let us examine the progress over the past year.

4.1.1 Photocathodes:

Two large fixed target experiments have demonstrated that both TEA and TMAE photocathodes are technologies that can be implemented. TMAE is rather more forgiving in terms of the allowable oxygen and water vapor contaminations, but seems to be chemically active and may cause poor electron drift lifetimes.

4.1.2 Optics:

The optics issue branches into two subheadings - 'photon optics' and 'electron transport optics.' The former is no special problem, only demanding a careful choice of mirror fabrication process and of the optimum geometry for a given experiment. The latter still needs work; electrons can be efficiently and uniformly transported over the desired drift lengths under the influence of static electric and magnetic fields. (Both the DELPHI and SLAC experiments demonstrate transport over 70 cms with distortion of less than 1 mm, in circumstances where positive ion charge effects are negligible.) However, distortions due to charge build up on the quartz boxes and the positive ion cloud need further study.

4.1.3 Detectors:

Several electrode geometries have been demonstrated to provide good single photoelectron detection efficiency, and have substantial protection against photon feedback. An additional factor of two rejection would be helpful, but is not absolutely required for an operational system. Studies have begun on the effect of $E \times B$ forces on detector efficiency, and will continue.

Third coordinate readout from both cathode coupled geometry and from charge division on resistive anodes have been demonstrated to give the required accuracy. Work will continue aggressively in this area.

4.1.4 Radiators

There were no special problems in the choice of radiators, beyond learning to keep them clean of oxygen and water vapor, both of which absorb strongly in the far U.V. region.

4.1.5 Engineering Considerations

Among the major problem areas in building new Čerenkov Ring Imaging Devices are: a) the choice of construction materials which will not react with TMAE or TEA, and which will not out-gas vapors which would absorb the Čerenkov photons or the photoelectrons, b) construction techniques which allow robust, economic assembly of devices without loss of coverage and c) imaginative and realistic geometric solutions which allow 4π coverage without compromising the possibility of servicing the device.

4.2 Summary of the Data

The measurements from the four groups working with ring imaging devices are summarized in Table II below.

Table II

Summary

Experiment	Radiator	Photocathode	Number of Photoelectrons			$N_0^{Achieved}/N_0^{Expected}$	Attenuation Length (cm)	$\Theta \pm \delta\Theta$ (mrad)	γ_{th}
			Detected	Zero Drift Length	Expected				
E-605	1500 cm [helium gas]	TEA	3	N.A.	6	25/50	N.A.	8.7 ± 0.09	116
RAL-Omega	500 cm [nitrogen gas]	TMAE	12	14	28	40/95	50	25.8 ± 0.5	41
DELPHI	1 cm [C_5F_{12} liquid]	TMAE	19	23	23	50/50	150-350 (> 500)	680 ± 80	1.5
	50 cm [isobutane gas]	TMAE	8	12	12	95/95	150-350 (> 500)	54.5 ± 3.0	17
SLD	1 cm [C_5F_{12} liquid]	TMAE	20	37	25	75/50	30-45	668 ± 90	1.5
	42 cm [isobutane gas]	TMAE	9	13	11	105/90	30-45	56.4 ± 3.2	17

4.3 Conclusions

- Čerenkov Ring Imaging Devices have been successfully used in two fixed target experiments at Fermilab and at the CERN SPS, demonstrating particle identification over a very large momentum range at high energy (*e.g.*, π/K separation at 3 σ level up to 200 GeV/c).
- Good progress has been achieved in the research and development efforts for the two 4π e^+e^- detectors at CERN and SLAC where the expected numbers of photoelectrons (12 from the gas, and 25 from the liquid radiators) have indeed been achieved (or even exceeded). The expected accuracy for the Čerenkov angle measurement has also been achieved.

It seems that the technique has come of age.....but there is a long hard path ahead on engineering and systems optimization before such devices can be implemented as "standard equipment."

REFERENCES

1. Sequinot J., and Ypsilantis T., Nucl. Inst. and Meth. 142, 377 (1977).

2. Ypsilantis T., Urban M., Seguinot J., and Ekelof T., "Spherical RICH in Weak Magnetic Field", Isabelle Proc. 973 (1981);

   Barrelet E., Seguinot J., Urban M., Ypsilantis T., "A Rich Detector", Isabelle Proc. 1378 (1981);

   "Delphi Technical Proposal" CERN-LEPC-83-03.

3. Ekelof T., Ypsilantis T., Sequinot J., and Tocqueville J., "The CRID: Recent Progress and Future Development", Phys. Scripta 23, 371 (1980).

   Williams S., Leith D., Poppe M., Ypsilantis T., "An Evaluation of Detectors for a CRID", IEEE, NS-27, 91 (1980);

   "SLD Design Report", SLAC Report 274 (1984).

4. Ash, W. et al., "SLD Design Report", SLAC Report 273 (1984).

5. Glass, H., et al., IEEE, NS-32, 692 (1985); IEEE, NS-30, 30 (1983). Adams, M. et al., Nucl. Inst. and Methods 217, 237 (1983).

6. Apsimon, R.J., et al., IEEE, NS-32, 674 (1985);

   Apsimon, R.J., et al., RAL Report 85-014.

7. "DELPHI Proposal", CERN/LEPC 83-3; "DELPHI Progress Report", CERN/LEPC 84-16.

8. Atwood, W., (private communication).